RSC Advances

PAPER

View Article Online
View Journal | View Issue



Cite this: *RSC Adv.*, 2022, **12**, 27987

# Enhancement of emission and luminescent thermal stability of $K_2SiF_6 : Mn^{4+}$ by synergy of co-doping with $Na^+$ and coating with GQDs†

Daishu Deng,[a] Yan Yu,[a] Tianman Wang,[a] Jun Lei,[a] Lin Wang,[a] Yuelan Li,[a] Sen Liao *[a] and Yingheng Huang*[b]

The luminescence properties and thermal stability of phosphors are key properties for practical applications. A series of $K_2SiF_6$: $Mn^{4+}$, $Na^+$ @ GQDs (KSF: $Mn^{4+}$, $Na^+$ @ GQDs, KSF = $K_2SiF_6$, GQDs = graphene quantum dots; here, Cl-contained graphene quantum dots are used) red light phosphors have been synthesized by using a combination of $H_2O_2$-free and hydrothermal coating methods. The fluorescence thermal stability and fluorescence intensity of the optimal phosphor are greatly improved by doping the matrix with $Na^+$ and coating it with GQDs. The strong negative thermal quenching (NTQ) effect and the color stability of the phosphor at variable temperatures result in good thermal stability. The strong NTQ effect is attributed to the phonon-induced transition mechanism. The high thermal stability makes the optimal sample ideal for high-power light LEDs (WLEDs). The test results show that the prototype WLED with the optimal sample as the red light component produces warm white light. The light has high luminescent efficiency (101.6 lm $W^{-1}$), low correlated color temperature (CCT = 3978 K), and high color rendering index ($R_a$ = 92.2).

Received 2nd September 2022
Accepted 23rd September 2022

DOI: 10.1039/d2ra05527a

rsc.li/rsc-advances



## 1. Introduction

White light emitting diodes (WLEDs) have become the new light source for displays and backlight fields in the 21st century because of their potential to reduce energy consumption and be environmentally friendly.[1,2] Currently, commercial WLEDs mainly consist of a yellow YAG : $Ce^{3+}$ phosphor and blue LED chip. These WLEDs produce a cool white light that is not suitable for practical applications due to their high correlated color temperature and low color rendering index drawbacks. The main reason for this is the lack of red light components in the prepared WLEDs, so research for red-emitting phosphors with high efficiency is necessary.[3,4] $Eu^{2+}$-doped nitride phosphors with good thermal and chemical stability have been used in commercial phosphors. These phosphors, when mixed with green/yellow phosphors, are proven to reabsorb. In addition, their emission spectrum bands are too broad and the main emission peak exceeds the sensitive region of the human eye, affecting the radiation luminescent efficiency of WLED devices. Fortunately, $Mn^{4+}$-doped fluoride phosphors have the advantage of narrow band emission, with high luminescence efficiency and color purity, which can be better suited for practical applications.[5,6]

Many studies of $Mn^{4+}$ doped fluoride phosphors have been reported. For example, the properties of $A_2MF_6 : Mn^{4+}$ (A = Li, Na, K, Rb, Cs; M = Ti, Ge, Si) phosphors have been studied.[7–18] However, poor fluorescence thermal stability is an inherent drawback of these phosphors, which may lead to a rapid decrease in their luminescence intensity due to thermal quenching at operating temperatures. To solve this problem, strategies such as surface coating, ion doping, and defect modification have been used.[19–22] It has been reported that the luminescence intensity of rare earth compounds can be increased by coating with carbon nanomaterials, such as reduced graphene oxychloride (rGO), graphite oxide (GO), and GQDs.[23–25] Among them, it is noteworthy that the long-range luminescence thermal stability of $SrBaSi_2O_2N_2 : Eu^{2+}$ is enhanced by coating with rGO. As seen from the above studies, coating the samples with GQDs is also an effective strategy in order to improve the thermal stability of the $Mn^{4+}$ doped phosphors.

In this paper, KSF: 0.06$Mn^{4+}$, 0.10$Na^+$ @ GQDs (10 mg $mol^{-1}$) with a strong NTQ effect was synthesized. The color temperature and display index of packaged WLED can meet the needs of practical applications, and it is an important candidate for future backlight and display applications.

[a]School of Chemistry and Chemical Engineering, Guangxi University, Nanning, Guangxi, 530004, China. E-mail: liaosen@gxu.edu.cn; huangyingheng@163.com; Fax: +86 771 3233718; Tel: +86 771 3233718

[b]School of Resources, Environment and Materials, Guangxi University, Nanning, Guangxi, 530004, China

† Electronic supplementary information (ESI) available. See https://doi.org/10.1039/d2ra05527a

Table 1 ICP element analysis results of samples (i–iii)

| No. | Na/% | K/% | Si/% | Mn/% | Atomic ratios of Na : K:Si : Mn | Calculated possible molecular formula |
|---|---|---|---|---|---|---|
| (i[a]) | 0.00 | 35.20 | 11.90 | 1.49 | 0.000 : 1.9975 : 0.9401 : 0.0602 | KSF: $0.06Mn^{4+}$ |
| (ii[b]) | 0.92 | 29.72 | 10.59 | 1.33 | 0.1000 : 1.9000 : 0.9412 : 0.0600 | KSF: $0.06Mn^{4+}$, $0.10Na^{+}$ |
| (iii[c]) | 0.92 | 29.73 | 10.58 | 1.32 | 0.1000 : 1.8993 : 0.9421 : 0.0605 | KSF: $0.06Mn^{4+}$, $0.10Na^{+}$ @ GQDs 10 mg $mol^{-1}$ |

[a] KSF: $0.06Mn^{4+}$. [b] KSF: $0.06Mn^{4+}$, $0.10Na^{+}$. [c] KSF: $0.06Mn^{4+}$, $0.10Na^{+}$ @ GQDs 10 mg $mol^{-1}$.

Table 2 Indexed results of the samples (i–iii)

| | $a = b = c$/Å | $\alpha = \beta = \gamma$/° | $V$ Å$^{-3}$ |
|---|---|---|---|
| PDF#75-0694 | 8.134 | 90 | 538.20 |
| (i[a]) | 8.13749 | 90 | 538.85 |
| (ii[b]) | 8.13428 | 90 | 538.22 |
| (iii[c]) | 8.13697 | 90 | 538.75 |

[a] KSF: $0.06Mn^{4+}$. [b] KSF: $0.06Mn^{4+}$, $0.10Na^{+}$. [c] KSF: $0.06Mn^{4+}$, $0.10Na^{+}$ @ GQDs 10 mg $mol^{-1}$.

## 2. Experimental and methodology

The contents of the experimental, methodology, mathematical calculation methods, and properties (Fig. S1–S6†) of GQDs (Cl-contained graphene quantum dots) are depicted in the ESI.†

## 3. Results and discussion

### 3.1. Structures, morphologies, and composition properties

It can be seen from Table 1 (ICP elemental analysis data) that possible molecular formulae of the three samples are as follows: (i) KSF: $0.06Mn^{4+}$, (ii) KSF: $0.06Mn^{4+}$, $0.10Na^{+}$, (iii) KSF: $0.06Mn^{4+}$, $0.10Na^{+}$ @ GQDs 10 mg $mol^{-1}$. The results show that $KMnO_4$ has been largely converted to $K_2MnF_6$ after 48 hours of reaction during the experiments and doped into the $K_2SiF_6$ matrix. The chemical reaction equations for synthesis the sample (i) are as follows:

$$4KMnO_4 + 4KF + 20HF = 4K_2MnF_6 + 10H_2O + 3O_2 \quad (1)$$

$$yK_2MnF_6 + (1 - y)K_2SiF_6 = K_2Si_{1-y}F_6 : yMn^{4+} \quad (2)$$

Eqn (1) shows the redox reaction of $KMnO_4$ in an acidic solution. Eqn (2) is the formation of KSF : $yMn^{4+}$ *via* ion exchange reaction.

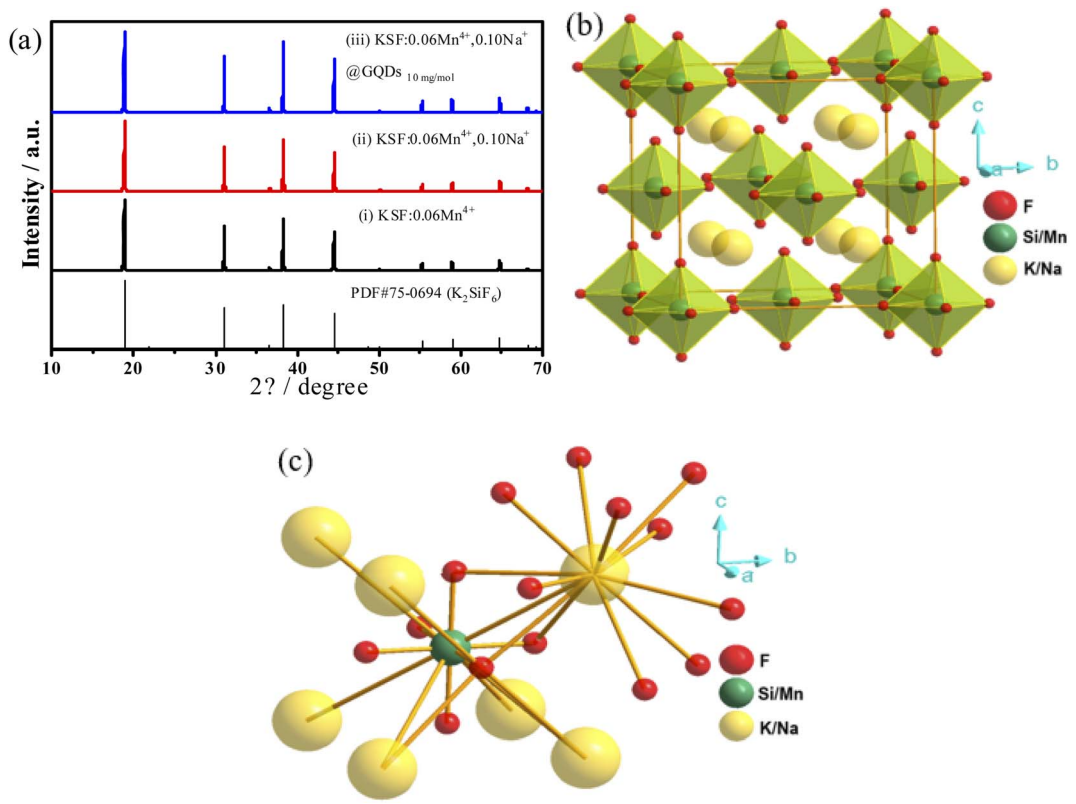


Fig. 1 (a) XRD patterns of the three samples: (i) KSF: $0.06Mn^{4+}$, (ii) KSF: $0.06Mn^{4+}$, $0.10Na^{+}$, (iii) KSF: $0.06Mn^{4+}$, $0.10Na^{+}$ @ GQDs 10 mg $mol^{-1}$, (b) The built unit cell structure of the sample (ii), (c) coordination environment surrounding Si/Mn.

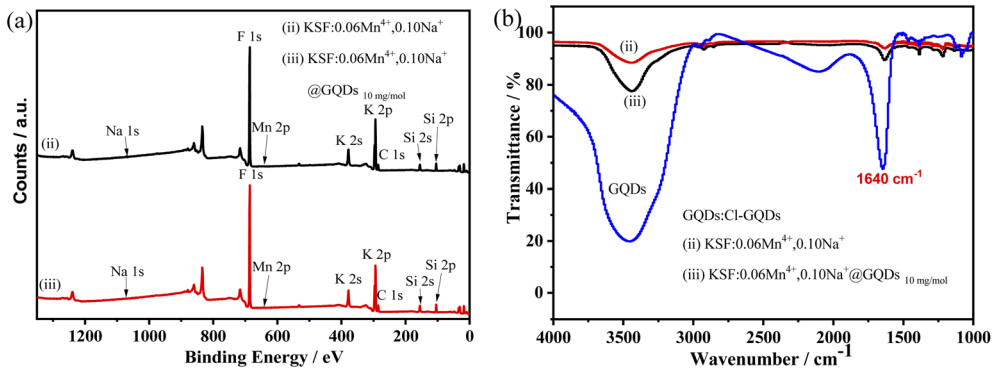


Fig. 2 XPS and FTIR spectra of samples, (ii) KSF: 0.06$Mn^{4+}$, 0.10$Na^{+}$, and (iii) KSF: 0.06$Mn^{4+}$, 0.10$Na^{+}$ @ GQDs 10 mg $mol^{-1}$ (a) XPS spectra, (b) FTIR spectra.

The XRD spectra of the samples (i)–(iii) are presented in Fig. 1a. The positions of diffraction peaks for the samples are consistent with the PDF#75-0694 standard data (the cubic $K_2SiF_6$ phase with a space group of Fm $\bar{3}$ m), suggesting the samples have high crystallinity. The indexed results are listed in Table 2. There are no peaks of GQDs in the sample (iii) because the mass content of GQDs is too small (~0.0045%) to be measured.

The results in Table 2 show that the lattice volumes of the samples are ranked as (i) > (iii) > (ii) > PDF#75-0694. The ionic radii (CN = 6) of $Na^{+}$, $K^{+}$, $Si^{4+}$, $Mn^{4+}$ are 1.18, 1.38, 0.40, 0.53 Å, respectively.[8,27,28] When $Mn^{4+}$ is doped into the $K_2SiF_6$ matrix, some $Si^{4+}$ in the lattice are replaced by $Mn^{4+}$, resulting in the lattice volume (i) of the sample slightly larger than that of PDF#75-0694. Similarly, when the smaller radius $Na^{+}$ replaces $K^{+}$ in the matrix, the lattice volume of the sample (ii) is slightly reduced compared to that of the sample (i). Furthermore, the GQDs coated on the sample (iii) are coordinated to $Mn^{4+}$ or $Si^{4+}$, leading to an increase in its lattice volume compared to the sample (ii). Fig. 1b shows the crystal structure of the sample (ii),

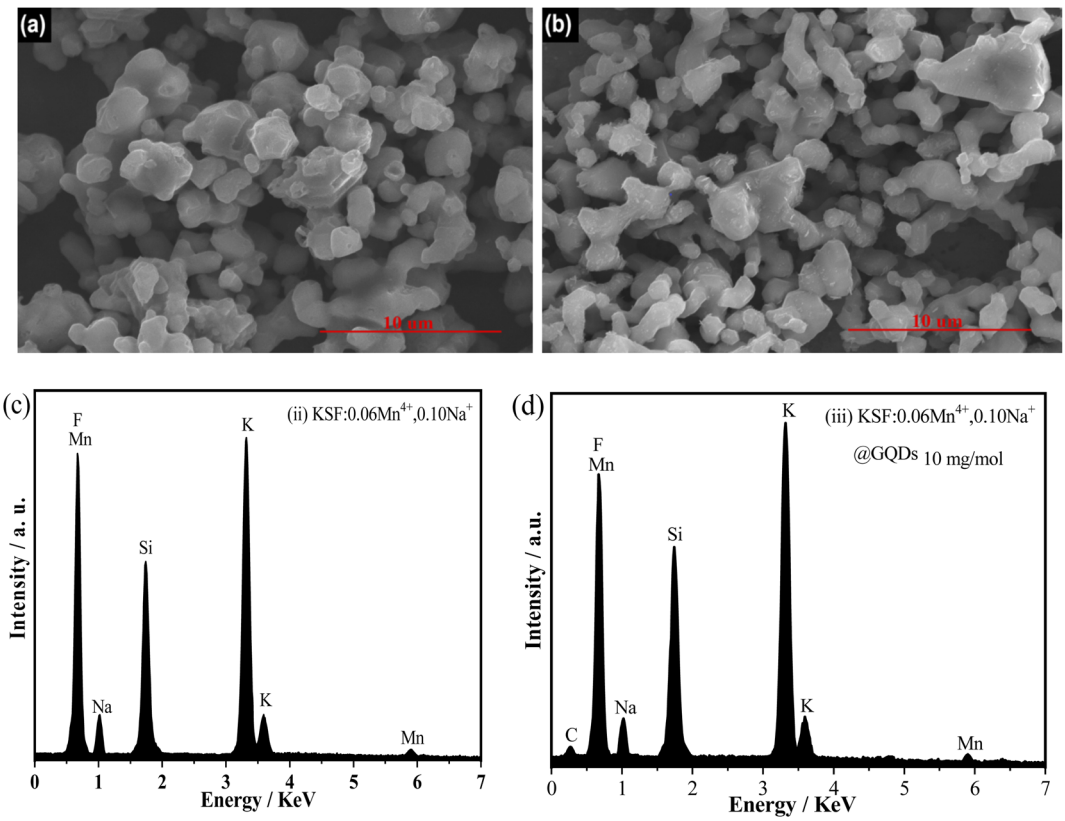


Fig. 3 SEM images and EDS spectra of two samples, (ii) KSF: 0.06$Mn^{4+}$, 0.10$Na^{+}$ and (iii) KSF: 0.06$Mn^{4+}$, 0.10$Na^{+}$ @ GQDs 10 mg $mol^{-1}$: (a and b) SEM images of sample (ii) and (iii) (c and d) EDS spectra.

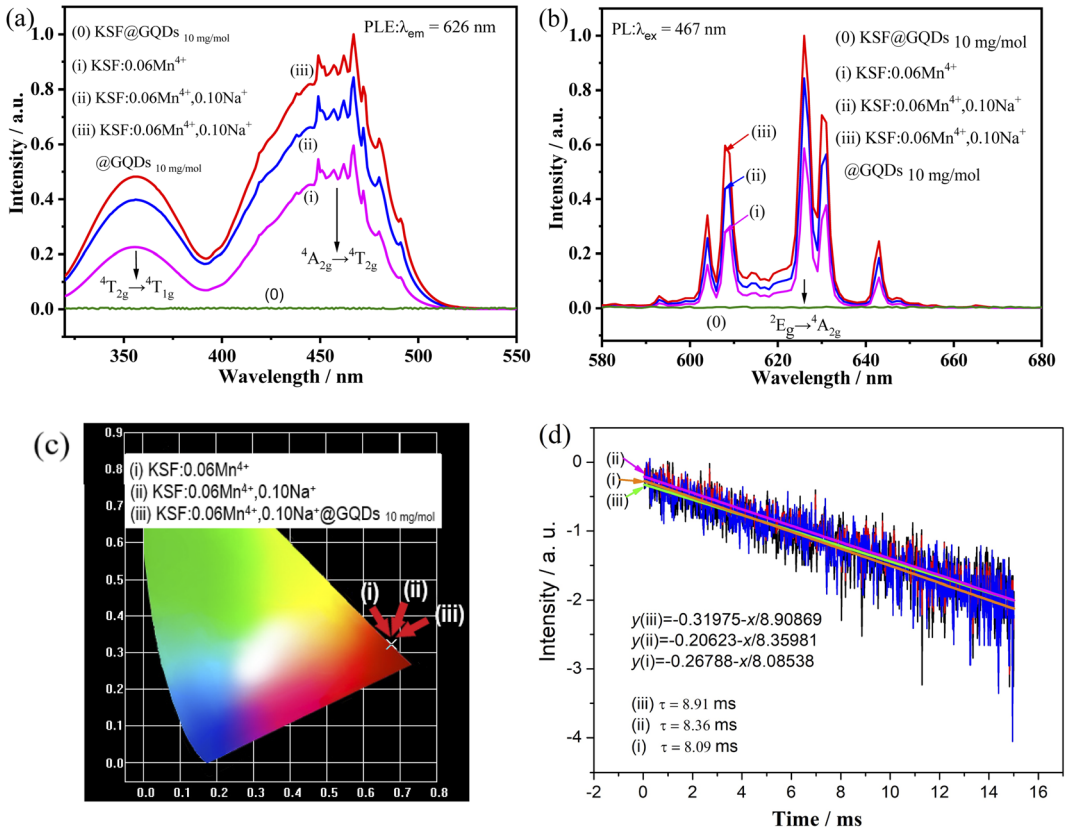


Fig. 4 Luminescent properties of four samples, (0) KSF @ GQDs 10 mg $mol^{-1}$, (i) KSF: 0.06$Mn^{4+}$, (ii) KSF: 0.06$Mn^{4+}$, 0.10$Na^{+}$, (iii) KSF: 0.06$Mn^{4+}$, 0.10$Na^{+}$ @ GQDs 10 mg $mol^{-1}$: (a) and (b) PLE and PL spectra, (c) CIE chromaticity diagram, (d) Lifetime curves of the samples (i–iii).

which belongs to the cubic crystal system and the Fm $\bar{3}$ m (225) space group. In this structure, there is only one type of octahedral $Si^{4+}$ ions (Fig. 1c).

Fig. 2 shows the XPS and FTIR spectra of the samples. In Fig. 2a, XPS depicts that the elements of the two samples (the samples (ii and iii)) are Na, K, Si, Mn, F, and C. The concentrations of $Mn^{4+}$ and $Na^{+}$ are very low, so the intensity of their peaks is not obvious. The FTIR spectra (Fig. 2b) shows that both the samples (ii and iii) have absorption peaks at 1640 $cm^{-1}$, but the intensity of the two peaks differs considerably, with that of the sample (iii) being much stronger than that of the sample (ii). The absorption peaks at 1640 and 3500 $cm^{-1}$ are probably from $H_2O$, while the stronger absorption of the sample (iii) at 1640 $cm^{-1}$ can be attributed to the overlapping peaks of the C=C vibrational peaks of the GQDs (Fig. S6†).[29]

Fig. 3 shows the EDS spectra and the SEM images of the samples (ii and iii). Fig. 3(a and b) show that the two samples consist of irregular lumpy particles of 2–5 μm in size, with the sample (iii) showing a clear agglomeration of particles. There are also some differences in the surfaces of the samples, with the sample (ii) having a smoother surface than that of the sample (iii). Fig. 3(c and d) illustrate that the sample (ii) consists of Na, K, Si, Mn, and F elements, and the elements Na, K, Si, Mn, F, and C appear in the sample (iii). The carbon peak (Fig. 3d) originates from the Cl-GQDs, however, no peak of Cl appears in the figure, probably because the chloride ions on the Cl-GQDs have been dissociated during the coating process. Based on the above results, it can be confirmed that the sample (iii) has been successfully coated with GQDs.

### 3.2. Luminescent properties at room temperature

The luminescent properties at room temperature of the samples ((0) KSF @ GQDs 10 mg $mol^{-1}$, (i) KSF: 0.06$Mn^{4+}$, (ii) KSF: 0.06$Mn^{4+}$, 0.10$Na^{+}$, (iii) KSF: 0.06$Mn^{4+}$, 0.10$Na^{+}$ @ GQDs 10 mg $mol^{-1}$) are shown in Fig. 4(a and b).

Fig. 4(a and b) show that no excitation or emission peaks are present in the sample (0), indicating that KSF @ GQDs 10 mg $mol^{-1}$ has no luminescence under blue light excitation, which is proven by Fig. 4b and S5.† The ratios of luminescence intensity of the samples (i)–(iii) in Fig. 4b are 1.00 : 1.44 : 1.70 respectively, indicating that fluorescence intensities of the samples are enhanced by doping with $Na^{+}$ and further increased after coating with GQDs. The luminescent intensity of the sample (iii) is 1.18 times that of the sample (ii). The luminescence enhancements by doping with $Na^{+}$ and coating with GQDs are also reported by Huang and Liu *et al.*[22,30] respectively.

As shown in Fig. 4(a and b), the excitation and emission peaks of these samples are in essentially the same position. In PLE spectra, there are two strong broad excitation bands centered at ~360 nm and ~460 nm, which belong to the spin-allowed $^4A_{2g} \rightarrow {}^4T_{1g}$ and $^4A_{2g} \rightarrow {}^4T_{2g}$ transitions of $Mn^{4+}$, respectively. The peaks in the PL spectrum occur in the 600–

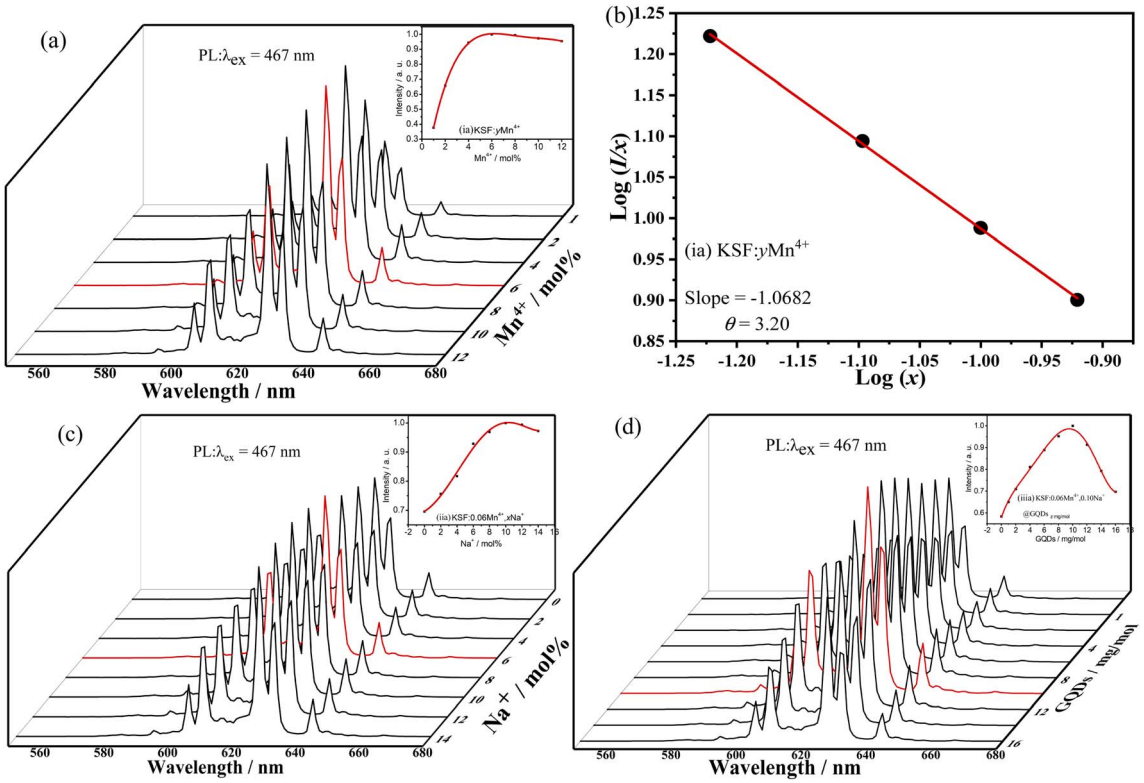


Fig. 5 The luminescent properties of three samples, (i-a) KSF : $y$Mn$^{4+}$, (ii-a) KSF: 0.06Mn$^{4+}$, $x$Na$^{+}$, (iii-a) KSF: 0.06Mn$^{4+}$, 0.10Na$^{+}$ @ GQDs z mg mol$^{-1}$: (a) and (c) and (d) PL spectra, (b) The related type line of multipolar interaction.

660 nm range, with the strongest peak at about 626 nm, which belongs to the $^2$Eg → $^4$A$_{2g}$ transition of Mn$^{4+}$ (spin forbidden d–d transition),[31,32] and it is activated by [MnF$_6$]$^{2-}$ vibronic modes.[33]

Internal quantum yield ($QY_i$) values of the samples (i)–(iii) are determined with the method described by some reports.[34] The $QY_i$ of the samples (i)–(iii) are determined to be 83.36, 86.80, and 99.97%, respectively. It is clear that $QY_i$ (92%) of K$_2$SiF$_6$ : Mn$^{4+}$ reported by Xie *et al.*[35] is smaller than that of the sample (iii).

It has been reported that $QY_i$ of K$_2$TiF$_6$ : Mn$^{4+}$ is larger than that of K$_2$SiF$_6$ : Mn$^{4+}$, and the former value is close to 100%.[34] This shows that the $QY_i$ of the samples can be improved by coating with GQDs.[36]

The chromaticity coordinates of the samples are obtained by using the emission spectra data in Fig. 4b. The calculated results are shown in Fig. 4c ((i) (0.6776, 0.3222), (ii) (0.6771, 0.3227), (iii) (0.6762, 0.3236)). The formula (eqn (S1)†) is used for calculating color purity.[37–39] The color purity of the samples (i–iii) are 99.70%, 99.84%, and 99.89% respectively, showing that the color purity of the sample coated with GQDs has been improved.

The luminescence decay curve of the sample can be well fitted by the linear equation (eqn (S3)†), which is transformed from eqn (S2):†[40] Fluorescence lifetime curves for the samples (i–iii) fitted with the eqn (S3)† are shown in Fig. 4d, and the lifetimes obtained from the curves are $\tau$ (i) = 8.91 ms, $\tau$ (ii) = 8.36 ms, $\tau$ (iii) = 8.09 ms, respectively. The results show that the lifetime is enhanced by doping of Na$^+$, then further improved by coating of GQDs. In contrast, the latter method has a greater enhancement effect than that of the former.

### 3.3. Luminescent properties of different samples

The influence of different molar ratios (atomic ratios) of Mn$^{4+}$ on the fluorescent performances of KSF : $y$Mn$^{4+}$ is shown in Fig. 5a. The curve first shows an increasing trend, reaching a maximum at 6% mol Mn$^{4+}$ doping concentration. Concentration quenching at higher concentrations leads to a decrease in fluorescence intensity.

The quenching mechanism of Mn$^{4+}$ concentration in KSF : $y$Mn$^{4+}$ is explored by the critical distance ($R_c$) between Mn$^{4+}$ ions. The $R_c$ is calculated from eqn (S4).†[39] For KSF: 0.06Mn$^{4+}$, $V$ = 538.22 Å$^3$ and $R_c$ is 23.42 Å. When $R_c$ is much larger than 5 Å, the quenching mechanism of the Mn$^{4+}$ concentration in KSF: 0.06Mn$^{4+}$ may be due to multipolar interactions rather than interactions. Eqn (S5)†[31,40] is used to estimate the multipolar interaction type for the sample. When $\theta$ are 6, 8, and 10, the corresponding mechanisms are the dipole–dipole, dipole–quadrupole, and quadrupole–quadrupole interactions, respectively. Fig. 5b shows that the slope of the KSF : $y$Mn$^{4+}$ straight line is −1.0682 and the value of $\theta$ is calculated as 3.20. Therefore, the quenching of the Mn$^{4+}$ concentration in the KSF : $y$Mn$^{4+}$ sample corresponds to the mechanism of dipole–dipole interactions.

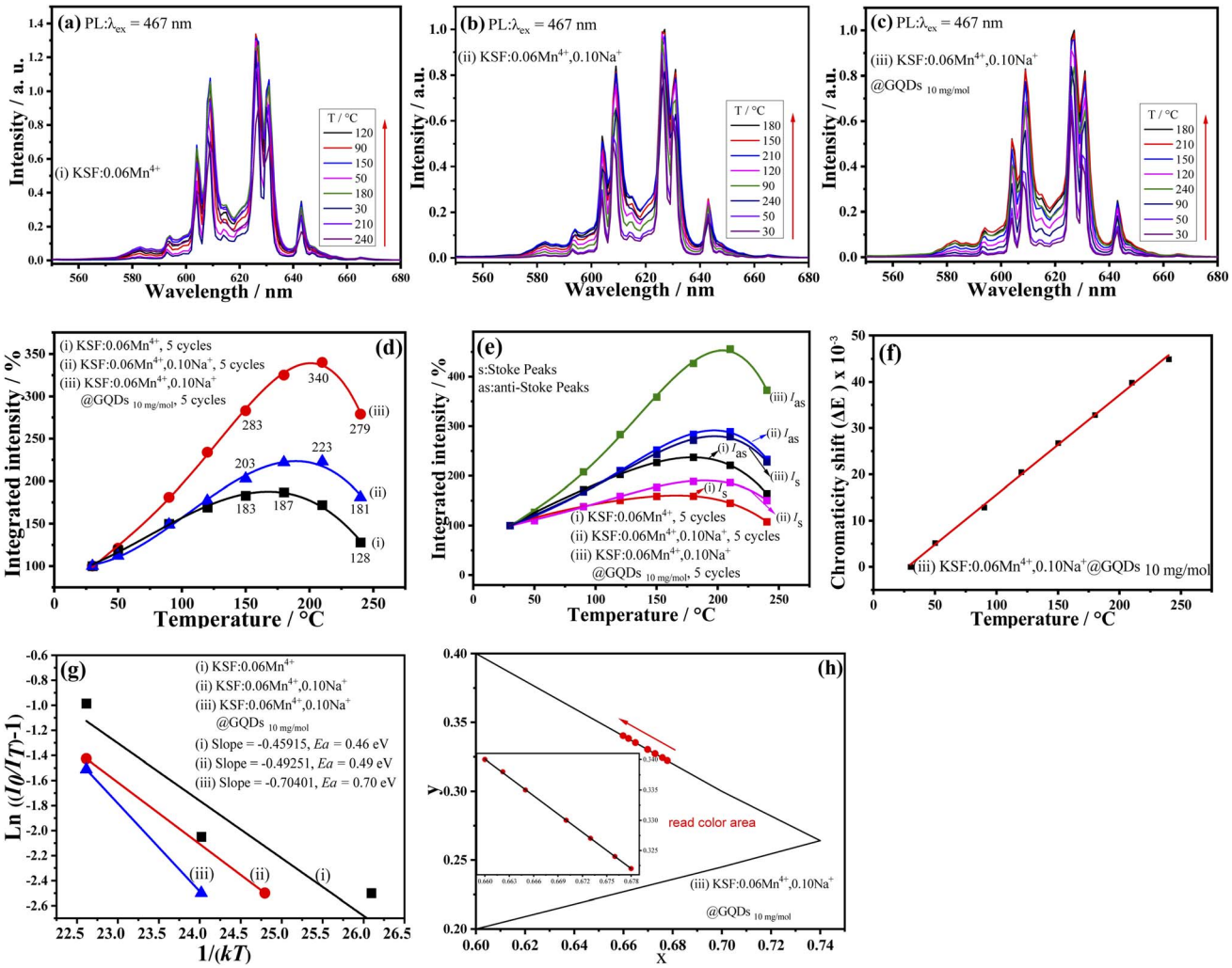


Fig. 6 Temperature-dependent PL performances of three samples, (i) KSF: 0.06$Mn^{4+}$, (ii) KSF: 0.06$Mn^{4+}$, 0.10$Na^{+}$, (iii) KSF: 0.06$Mn^{4+}$, 0.10$Na^{+}$ @ GQDs 10 mg $mol^{-1}$: (a) and (b) and (c) PL spectra; (d) Integrated intensity curves; (e) Integrated intensity curves of Stoke and anti-Stoke peaks, (f) Chromaticity shift of sample (iii), (g) $E_a$ curves, (h) CIE color coordinates of sample (iii).

Based on KSF: 0.06$Mn^{4+}$, the effect of doping with different $Na^{+}$ concentrations on the fluorescence properties of KSF: 0.06$Mn^{4+}$, $x$$Na^{+}$ is shown in Fig. 5c. The influence curve is a parabola one with a maximum value. First, the curve goes up with the increase of $x$, and achieves a maximum value at $x$ = 10%, then declines when $y$ surpasses 10% due to the concentration quenching.

The influence of different coating concentrations of GQDs on the luminescent properties of KSF: 0.06$Mn^{4+}$, 0.10$Na^{+}$ @ GQDs z mg $mol^{-1}$ was also investigated (Fig. 5d). The influence curve is nonlinear with a maximum value. First, the curve goes up with the increase of $z$, and achieves a maximum value at $z$ = 10 mg $mol^{-1}$, then it decreases when $z$ exceeds 10 mg $mol^{-1}$ due to concentration quenching.

### 3.4. Analyses of thermal performances

The fluorescence property changes with temperature is critical for WLEDs applications, due to the working temperature of WLEDs can reach about 150 °C. Fig. 6 shows the relationship

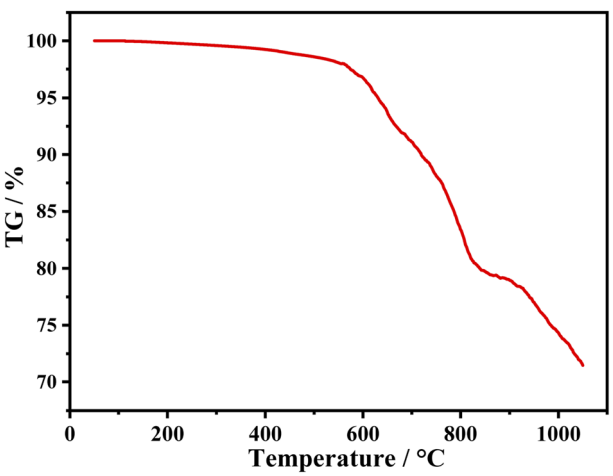


Fig. 7 TG of sample, (iii) KSF: 0.06$Mn^{4+}$, 0.10$Na^{+}$ @ GQDs 10 mg $mol^{-1}$.

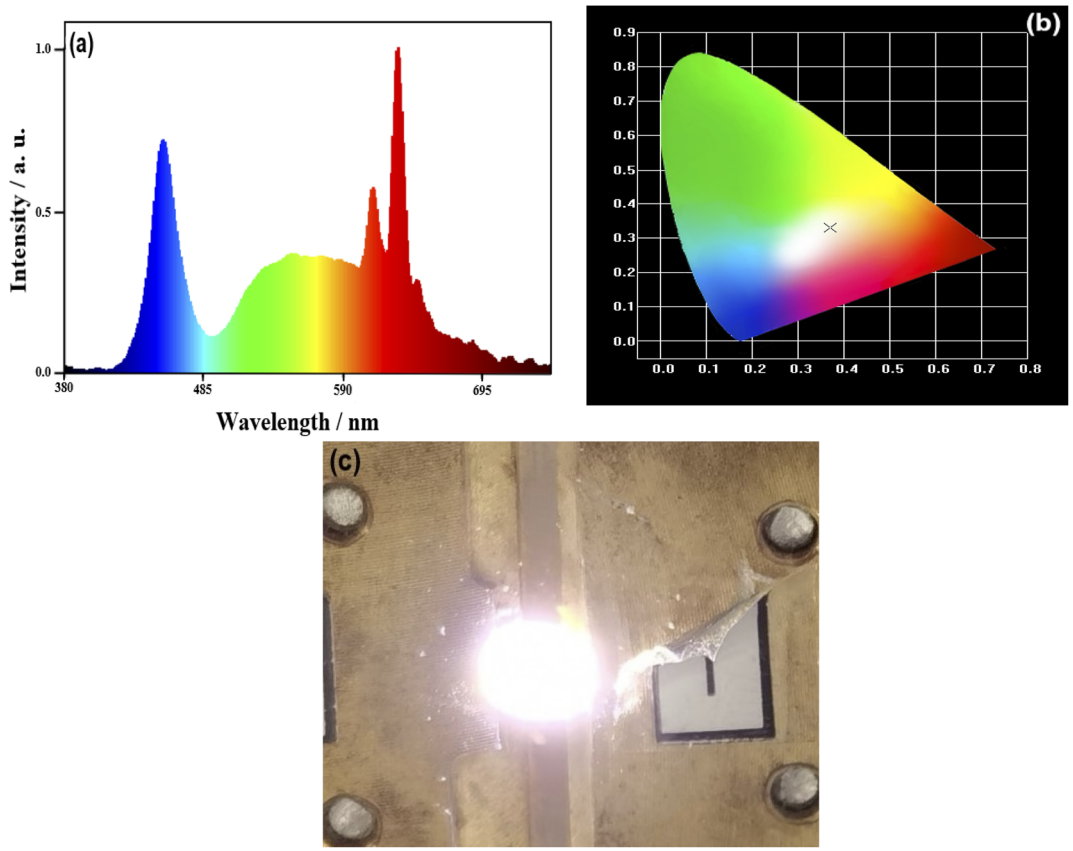


Fig. 8 Performances of prototype WLEDs using the mixing phosphors of KSF: 0.06$Mn^{4+}$, 0.10$Na^{+}$ @ GQDs 10 mg $mol^{-1}$ and YAG : $Ce^{3+}$ based on InGaN chip under a 20 mA drive current: (a) Electroluminescence spectra, (b) CIE chromaticity diagram, (c) A photograph of the white emission spectrum of the driven LED.

between luminescence intensities of the samples (i–iii) and temperatures. Fig. 6a–c illustrate that the luminescence intensities of the three samples are strongly affected by temperature, but no emission shifts with increasing temperature.

The relationship curves between integrated luminescence intensities of the samples and temperatures are parabola curves with their maximum values (Fig. 6d), which are analogous to that of $K_3AlF_6 : Mn^{4+}$ reported by Tang *et al.*[20] First, with the increase of temperatures, the curves increase and achieve their maximum values at 180, 210, and 210 °C for the samples (i–iii), respectively. Meanwhile, Fig. 6d shows a NTQ effect for the three samples, and the luminescence intensity curves remain essentially constant after five cycles of testing (30–240 °C). The results of Fig. 6d indicate that the luminescent and chemical thermal stability of the sample are excellent. But the three curves of Fig. 6d have some differences. In contrast, the values of the three curves at 180, 210, and 240 °C are as follows: (a) 325, 340, and 279% for the sample (iii); (b) 222, 223, and 181% for the sample (ii); and (c) 187, 172, and 128% for the sample (i). So, the above results show that the three samples have high luminescence thermal stability. It can be seen that: (a) First, $K_2SiF_6 : yMn^{4+}$ obtained *via* the preparing method of this paper has the NTQ effect; (b) Second, after doping of $Na^{+}$, the NTQ is obviously enhanced; (c) The NTQ is further enhanced by the coating of GQDs. As mentioned above, several $Mn^{4+}$-doped phosphors prepared *via* various methods have the NTQ behavior.[19–21] But, in most cases, they do not have the NTQ. The results of this paper and our previous work show that coating with GQDs is an effective method to synthesize red-emitting phosphors with the NTQ.[22,26]

Fig. 6e shows relationship curves between $W_a$, $W_s$ of the samples (i–iii) and temperatures (here, $W_a$, and $W_s$ are integrated intensities of anti-Stokes peaks and Stokes peaks, respectively). The curves are used to study the NTQ mechanism. Fig. 6e shows that curves of $W_a$ and $W_s$ are nonlinear curves with highest points, but the height of the former is greater than that of the latter, for every sample. When the temperatures are 180, 210, and 210 °C, the curves of the samples (i–iii) reach their maximum values, respectively. These NTQ behaviors of the anti-Stokes and the Stokes transitions can be expressed with eqn (S6a and S7).†[36]

Eqn (S6 and S7)† show that the $W_a$ and $W_s$ are increased with increasing temperatures. In addition, eqn (S6 and S7)† also indicate that the former can be enhanced faster than the latter with increasing temperature. The curve trend of Fig. 6e coincides with that of Fig. 6d.

Eqn (S6 and S7)† indicate that the increase in radiative transition probability induced by the phonon is greater than that of the non-radiative one, which may be used to explain the NTQ effect of the three samples. In conclusion, with the help of

the phonon-induced transition, some of the heat energy is changed into luminous energy, resulting in the NTQ effect.

In addition, due to their large conjugated -bonds, GQDs can coordinate with $Mn^{4+}$ as electron donors, resulting in a greater NTQ effect in the sample (iii) than in the samples (i) and (ii).

$\Delta E$ (chromaticity shift) at different temperatures is calculated with eqn (S8).†[41,42] The smaller $\Delta E$ value means better color stability. Fig. 6f shows the $\Delta E$ values for the sample (iii) at different temperatures, and the curve is basically a straight line. According to the curve, $\Delta E$ is very small before 175 °C ($\Delta E = 31.98 \times 10^{-3}$). By comparison, the $\Delta E$ of a commercial red-emitting phosphor ($CaAlSiN_3 : Eu^{2+}$ (CSASNE)) at 175 °C is as high as $44 \times 10^{-3}$,[44] indicating the sample (iii) has good luminescence thermal stability for practical applications.

$E_a$ (activation energy) of the phosphor is an important parameter in evaluation of thermal stability. The higher the activation energy is, the better the fluorescence thermal stability of the sample is. Eqn (S9)† is applied to calculate the $E_a$ of the luminescent thermal quenching. Eqn (S10)† can be transformed from eqn (S9).†[43,44]

Calculated results of $E_a$ values for the samples (i–iii) from eqn (S10)† are shown in Fig. 6g, which are 0.46, 0.49, and 0.70 eV, respectively. As a result, sample (iii) has the best fluorescence thermal stability.

Fig. 6h shows the trend of color coordinates of the sample (iii) at different temperatures, and it has a small shift in color coordinates, which may be due to the slight widening of emission peaks, suggesting it has good color stability.

TG curve of the sample (iii) is shown in Fig. 7. There is only 0.17% weight loss before 200 °C, which is attributed to volatilization of adsorbed water. Significant weight loss occurs at around 600 °C, indicating that it has good chemical thermal stability.

### 3.5. Performances of prototype WLED

In order to test practical application of the sample (iii), the sample (iii), $YAG : Ce^{3+}$ and epoxy are mixed into a paste in proportion and coated on an InGaN chip to obtain an assembled prototype WLED. The electroluminescent properties of the WLED driven by a 20 mA current are shown in Fig. 8. Fig. 8a shows the electroluminescence spectrum of the WLED. The chromaticity coordinates of the WLED are (0.3694, 0.3304) (Fig. 8b), and the corresponding CCT is 3978 K. Besides, luminescent efficiency and $R_a$ obtained from the performance test are 101.6 lm $W^{-1}$ and 92.2, respectively. A luminescent photo of the WLED is illustrated in Fig. 8c, and it shows warm white light. Therefore, WLEDs with the sample (iii) as the red light component can meet the needs of practical applications.

## 4. Conclusions

In summary, $KSF : Mn^{4+}$, $Na^+$ @ GQDs phosphors were synthesized by a combination of the $H_2O_2$-free method and hydrothermal coating method, where the best sample was KSF: $0.06Mn^{4+}$, $0.10Na^+$ @ GQDs 10mg $mol^{-1}$. The fluorescence thermal stability and luminescence intensity of the phosphor were simultaneously enhanced by doping with $Na^+$ and coating with GQDs: (a) The luminescent intensity ratios of the samples (i–iii) ((i)KSF: $0.06Mn^{4+}$, (ii) KSF: $0.06Mn^{4+}$, $0.10Na^+$, (iii) KSF: $0.06Mn^{4+}$, $0.10Na^+$ @ GQDs 10 mg $mol^{-1}$) are 1.00 : 1.44 : 1.70; (b) the samples (i–iii) all have the NTQ effect, with the most pronounced effect in the sample (iii). The test results show that the sample (iii) has both fluorescence thermal stability and chemical thermal stability at the operating temperature (about 150 °C). A warm white light (luminescence efficiency = 101.6 lm $W^{-1}$, CCT = 3978 K, and $R_a$ = 92.2) was obtained for the assembled WLED prototype driven by a 20 mA current, indicating that the sample can be used as a high-power warm white light with good prospects applications in display and backlight filed.

## Author contributions

Daishu Deng: methodology, formal analysis, investigation, writing – original draft. Yan Yu: investigation. Tianman Wang: investigation. Jun Lei: investigation. Lin Wang: investigation. Lin Wang: conceptualization, supervision. Yuelan Li: review & editing, visualization. Sen Liao: review & editing, visualization. Yingheng Huang: review & editing, visualization.

## Conflicts of interest

The authors declare no conflict of interest.

## Acknowledgements

This research is supported by the National Natural Science Foundation of China (Grant No. 21661006 and No. 21965004), the Natural Science Foundation of Guangxi Zhuang Autonomous Region, China (Grant No. 2019GXNSFDA245022, No. 2020GXNSFAA159036), the Scientific Research Foundation of Guangxi University (Grant No. XDZ140116), the innovation Project of Guangxi Graduate Education (Grant No. YCSW2020015), the Students Experimental Skills and Innovation Ability Training Fund Project of Guangxi University (No. S202210593143).

## References

1 D. Q. Chen, W. D. Xiang, X. J. Liang, J. S. Zhong, H. Yu, M. Y. Ding, H. W. Lu and Z. G. Ji, *J. Eur. Ceram. Soc.*, 2015, **35**, 859–869.
2 J. H. Li, J. Yan, D. W. Wen, W. U. Khan, J. X. Shi, M. M. Wu, Q. Su and P. A. Tanner, *J. Mater. Chem. C*, 2016, **4**, 8611–8623.
3 Y. C. Lin, M. Karlsson and M. Bettinelli, *Top. Curr. Chem.*, 2016, **37**, 21.
4 M. M. Shang, J. Fan, H. Z. Lian, Y. Zhang, D. L. Geng and J. Lin, *Inorg. Chem.*, 2014, **53**, 7748–7755.
5 D. Q. Chen, Y. Zhou and J. S. Zhong, *RSC Adv.*, 2016, **6**, 86285–86296.
6 S. Ye, F. Xiao, Y. X. Pan, Y. Y. Ma and Q. Y. Zhang, *Mater. Sci. Eng., R*, 2010, **71**, 1–34.

7 L. Huang, Y. Liu, S. C. Si, M. G. Brik, C. X. Wang and J. Wang, *Chem. Commun.*, 2018, **54**, 11857–11860.
8 L. Huang, Y. Liu, J. B. Yu, Y. W. Zhu, F. J. Pan, T. T. Xuan, M. G. Brik and C. X. Wang, *ACS Appl. Mater. Interfaces*, 2018, **10**, 18082–18092.
9 H. Jia, L. Cao, Y. Wei, H. Q. Wang, H. Xiao, G. G. Li and J. Lin, *J. Alloys Compd.*, 2018, **738**, 307–316.
10 S. Sakurai, T. Nakamura and S. Adachi, *Jpn. J. Appl. Phys.*, 2018, **57**, 022601.
11 T. Senden, R. J. A. van Dijk-Moes and A. Meijerink, *Light: Sci. Appl.*, 2018, **7**, 8.
12 Y. W. Zhu, D. Q. Chen, L. Huang, Y. Liu, M. G. Brik, J. S. Zhong and J. Wang, *J. Mater. Chem. C*, 2018, **6**, 3951–3960.
13 Y. Jin, M. H. Fang, M. Grinberg, S. Mahlik, T. Lesniewski, M. G. Brik, G. Y. Luo, J. G. Lin and R. S. Liu, *ACS Appl. Mater. Interfaces*, 2016, **8**, 11194–11203.
14 S. J. Qiu, H. W. Wei, M. M. Wang, S. Zhang, Y. Zhou, L. Xu, X. M. Wang and H. Jiao, *RSC Adv.*, 2017, **7**, 50396–50402.
15 Z. L. Wang, Y. Liu, Y. Y. Zhou, Q. Zhou, H. Y. Tan, Q. H. Zhang and J. H. Peng, *RSC Adv.*, 2015, **5**, 58136–58140.
16 Z. L. Wang, Y. Y. Zhou, Z. Y. Yang, Y. Liu, H. Yang, H. Y. Tan, Q. H. Zhang and Q. Zhou, *Opt. Mater.*, 2015, **49**, 235–240.
17 M. M. Zhu, Y. X. Pan, X. A. Chen, H. Z. Lian and J. Lin, *J. Am. Ceram. Soc.*, 2018, **101**, 4983–4993.
18 Y. W. Zhu, S. Yuan, L. Huang, Y. Liu, X. Y. Li, J. S. Zhong, Y. F. Chen, D. Q. Chen and J. Wang, *Dalton Trans.*, 2019, **48**, 711–717.
19 H. D. Nguyen, C. C. Lin and R. S. Liu, *Angew. Chem., Int. Ed.*, 2015, **54**, 10862–10866.
20 X. Tang, X. D. Li, Z. H. Zou, Z. D. Ma, J. C. Zhang, Z. Z. Wang, Z. P. Ci, D. Y. Wang, S. L. Peng, H. H. Li and Y. H. Wang, *J. Mater. Chem. C*, 2017, **5**, 10369–10374.
21 Y. Y. Zhou, E. H. Song, T. T. Deng, Y. J. Wang, Z. G. Xia and Q. Y. Zhang, *Adv. Mater. Interfaces*, 2019, **6**, 1802006.
22 T. C. Lang, J. Y. Wang, T. Han, M. S. Cai, S. Q. Fang, Y. Zhong, L. L. Peng, S. X. Cao, B. T. Liu, E. Polisadova, V. Korepanov and A. Yakovlev, *Inorg. Chem.*, 2021, **60**, 1832–1838.
23 A. K. Srivastava, V. Gupta, C. S. Yerramalli and A. Singh, *Composites, Part B*, 2019, **179**, 107539.
24 W. J. Zhang, X. F. Zou and J. F. Zhao, *J. Mater. Chem. C*, 2015, **3**, 1294–1300.
25 G. Anoop, J. R. Rani, J. Lim, M. S. Jang, D. W. Suh, S. Kang, S. C. Jun and J. S. Yoo, *Sci. Rep.*, 2016, **6**, 33993.
26 Y. L. Li, X. Zhong, Y. Yu, Y. M. Liu, S. Liao, Y. H. Huang and H. X. Zhang, *Mater. Chem. Phys.*, 2021, **260**, 124149.
27 Y. Gao, Q. W. Long, R. Nong, T. M. Wang, Y. H. Huang, S. Liao and H. X. Zhang, *J. Electron. Mater.*, 2016, **46**, 911.
28 Y. M. Liu, T. M. Wang, Z. P. Chen, K. Y. Chen, M. M. Guan, Y. H. Huang, S. Liao and H. X. Zhang, *J. Mater. Sci.: Mater. Electron.*, 2018, **29**, 12536–12542.
29 Y. C. Zhao, L. J. Huang, Y. X. Wang, J. G. Tang, Y. Wang, J. X. Liu, L. A. Belfiore and M. J. Kipper, *J. Alloys Compd.*, 2016, **687**, 95–113.
30 S. Y. Wang, Q. Sun, B. Devakumar, J. Liang, L. L. Sun and X. Y. Huang, *J. Lumin.*, 2019, **214**, 116525.
31 M. G. Brik, S. J. Camardello and A. M. Srivastava, *ECS J. Solid State Sci. Technol.*, 2014, **4**, R39.
32 Y. M. Liu, Y. L. Li, W. J. Huang, J. M. Meng, W. F. Liang, S. Liao, Y. H. Huang and H. X. Zhang, *J. Mater. Sci.: Mater. Electron.*, 2019, **30**, 14646–14656.
33 L. P. Dong, L. Zhang, Y. C. Jia, B. Q. Shao, W. Lü, S. Zhao and H. P. You, *ACS Sustainable Chem. Eng.*, 2020, **8**, 3357–3366.
34 J. C. D. Mello, H. F. Wittmann and R. H. Friend, *Adv. Mater.*, 2010, **9**, 230.
35 Z. Y. Hou, X. Y. Tang, X. F. Luo, T. L. Zhou, L. Zhang and R. J. Xie, *J. Mater. Chem. C*, 2018, **6**, 2741–2746.
36 H. M. Zhu, C. C. Lin, C. W. Q. Luo, S. T. Shu, Z. G. Liu, Y. S. Liu, J. T. Kong, E. Ma, Y. G. Cao, R. S. Liu and X. Y. Chen, *Nat. Commun.*, 2014, **5**, 5312.
37 L. Y. Wang, E. H. Song, Y. Y. Zhou, T. T. Deng, S. Ye and Q. Y. Zhang, *J. Mater. Chem. C*, 2017, **5**, 7253–7261.
38 W. T. Xu, Y. F. Zhou, D. C. Huang, M. Y. Su, K. Wang, M. Xiang and M. C. Hong, *J. Mater. Chem. C*, 2015, **3**, 2003–2015.
39 M. M. Zhu, Y. X. Pan, L. Q. Xi, H. Z. Lian and J. Lin, *J. Mater. Chem. C*, 2017, **5**, 10241–10250.
40 M. G. Brik, S. J. Camardello, A. M. Srivastava, N. M. Avram and A. Suchocki, *ECS J. Solid State Sci. Technol.*, 2015, **5**, R3067.
41 X. J. Zhang, L. Huang, F. J. Pan, M. M. Wu, J. Wang, Y. Chen and Q. Su, *ACS Appl. Mater. Interfaces*, 2014, **6**, 2709–2717.
42 X. J. Zhang, J. Wang, L. Huang, F. J. Pan, Y. Chen, B. F. Lei, M. Y. Peng and M. M. Wu, *ACS Appl. Mater. Interfaces*, 2015, **7**, 10044–10054.
43 Y. W. Zhu, L. Huang, R. Zou, J. H. Zhang, J. B. Yu, M. M. Wu, J. Wang and Q. Su, *J. Mater. Chem. C*, 2016, **4**, 5690–5695.
44 Y. W. Zhu, L. Y. Cao, M. G. Brik, X. J. Zhang, L. Huang, T. T. Xuan and J. Wang, *J. Mater. Chem. C*, 2017, **5**, 6420–6426.